Received: 13 July 2022 | Revised: 11 January 2023 | Accepted: 22 January 2023

DOI: 10.1002/mop.33647

RESEARCH ARTICLE

WILEY

A compact fully fabric I-shaped antenna supported with textile-based AMC for low SAR 2.45 GHz wearable applications

Omar M. Youssef[1] | **Mohamed El Atrash**[1] | **Mahmoud A. Abdalla**[2]

[1]Electronics Systems Engineering, October University for Modern Sciences and Arts, Giza, Egypt

[2]Department of Electronic Engineering, MTC College, Cairo, Egypt

Correspondence
Mohamed El Atrash, Electronics Systems Engineering, October University for Modern Sciences and Arts, Giza 12573, Egypt.
Email: mzaky@msa.eun.eg

Abstract

Introduced in this letter is a thin, flexible, compact, and fully fabric I-shaped quarter-wavelength antenna, where a 3×3 array reflector, is in the antenna rear end. In free space, the I-shaped antenna radiates at 2.45 GHz of the Industrial, Scientific, and Medical band with simulated realized gain of 1.65 dB and 90% worth of simulated radiation efficiency. The array reflector is utilized to diminish the specific absorption rate (SAR) in human evaluation scenarios. At the operating frequency, in free space, the antenna realized gain is improved by 75% after incorporating the artificial magnetic conductor (AMC) array. Moreover, over 1 g of tissue, a SAR reduction of 99.5% is attained at 2.45 GHz. Simulation and measured S_{11} and radiation pattern comparisons are highlighted in this letter. Based on the accomplished outcomes, the integrated antenna, comprised of the fully fabric I-shaped quarter-wavelength antenna and the AMC array, might be considered for wearable applications.

KEYWORDS

compact antenna, fully fabric-based antenna, ISM applications, low SAR, wearable applications

1 | INTRODUCTION

Over the years, wireless body area network (WBAN) research have been in continuous development. Wearable devices enter into many applications such as sports, medical, and emergency rescue missions. The WBANs include on-body and off-body sensors that can be used for such applications, where the wearer is tracked and data are collected. Subsequently, they are transmitted via the wearable antenna to be analyzed. In medical applications, the wearer can be saved by monitoring his/her health conditions on daily basis.[1] Wearable antennas operate within the vicinity of the human body, where body-centric communications occur. On-body communication highlights the wireless communication link created in the middle of various human-mounted devices. In contrast, off-body communication refers to the wireless communication link between the body-worn device and the base station antenna.[1] The Industrial, Scientific, and Medical (ISM) band is the most appropriate band, due to its privileges pertaining to being license-free and dedicated to medical applications with sufficient bandwidth.

Traditional antennas are rigid and present uncomfortable feeling; however, body-worn antennas need certain properties such as flexibility; hence, this type of antenna is designed on substrates, which are based on soft materials. Substrates like polyethylene, polycarbonate and polyester sheets,[2,3] textile,[4–11] polydimethylsiloxanes (PDMS),[12,13] and thin polyimides[14–16] are flexible and robust. These substrates made flexible electronics more attractive than conventional electronics technology.

A lot of research have been published with a focus on specific absorption rate (SAR) reduction. It is governed by two main standards. The first is the American one, where its threshold level is 1.6 W/kg averaging over 1 g of tissue, while the second is the European one, which has a threshold limit of 2 W/kg averaging over 10 g of tissue. The SAR value can be decreased by widening the void space between the antenna and human body,[16] designing reflectors in the form of arrays,[2–9,11,12,14–17] that are relatively large in size, or having a full ground plane separator.[13] These structures are usually placed in the void space between the antenna and human body; therefore, reflecting the back radiations to a normal direction from the human body.

Accordingly, presented in this letter is a thin and low-footprint antenna, which is based on fabric materials to ensure flexibility and compatibility with human clothes. It is backed with a 3×3 artificial magnetic conductor (AMC) array to ensure that the human body is protected against unsafe radiations.

2 | THE PROPOSED ANTENNA CONFIGURATION AND FREE-SPACE PERFORMANCE

In this section, the antenna evolution is highlighted along with the outcome of each design step, leading to the proposed I-shaped antenna that operates at 2.45 GHz of the ISM band. Afterward, the proposed antenna layout is presented along with its performance in free space.

The proposed I-shaped quarter-wavelength radiator is made of the conductive textile ShieldIt with a conductivity and thickness of 1.8×10^5 S/m and 0.17 mm, respectively. It has equal width and length of 28 mm (0.228λ). The radiator is mounted on a substrate of felt with relative permittivity = 1.2, a 1.5 mm of thickness, and a tangent loss of 0.044. The radiator is fed using the coplanar waveguide (CPW) feeding technique which is made of ShieldIt Super too. Displayed in Figure 1 is the step-by-step methodology leading to the proposed I-shaped antenna. First, a conventional quarter-wavelength square monopole antenna (Case 1) was designed, as shown in Figure 1A. The equivalent circuit of the monopole is a series resonator, as shown in Figure 2A, where the equivalent inductance and capacitance are equivalent to a quarter wavelength resonator. The initial length of the square monopole was designed such that it equals 28 mm according to Equation (1).

$$D = \frac{3 \times 10^8}{4\sqrt{\varepsilon_r} f} \quad (1)$$

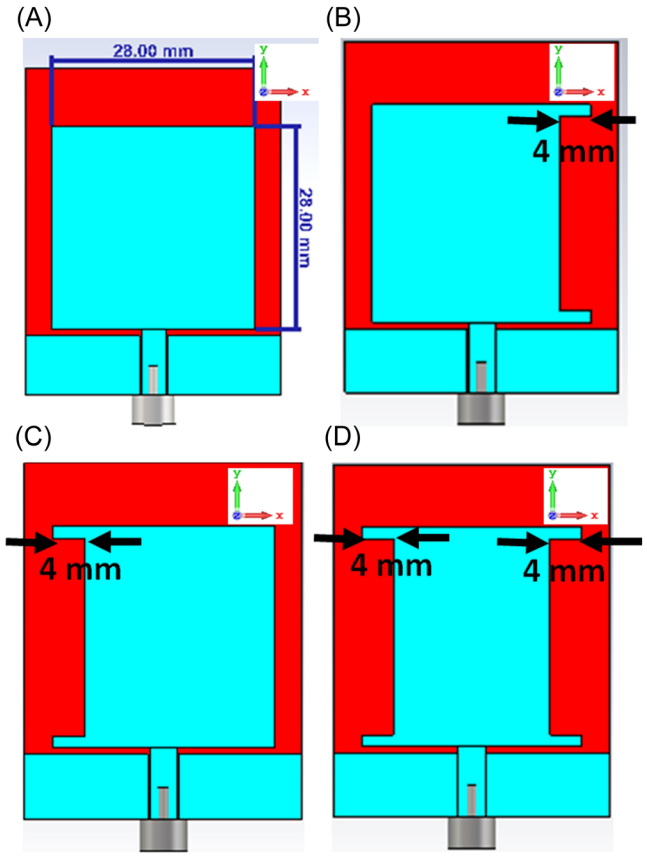

FIGURE 1 Step-by-step methodology of the antenna design: (A) the conventional square-shaped monopole antenna (Case 1); (B) etched right slot antenna (Case 2); (C) etched left slot antenna (Case 3); and (D) the I-shaped antenna (Case 4).

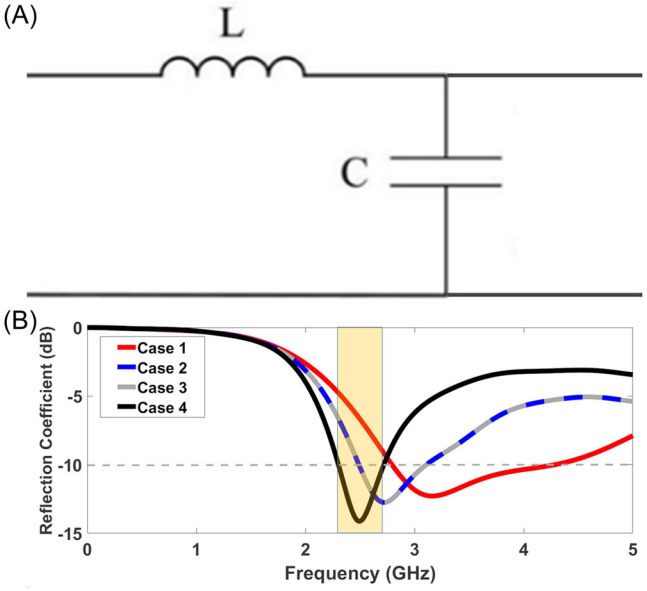

FIGURE 2 (A) The square monopole antenna equivalent circuit model of a series resonator. (B) Comparison between each antenna design step reflection coefficient.

As a verification, this antenna was simulated using the CST EM simulator and its simulated reflection is plotted in Figure 2B, where the antenna in this case resonates at 3.16 GHz. It is evident that it operates at a different frequency from 2.45 GHz (the desired frequency), as a fact of the effect of simplified formula in Equation (1). However, it can be considered a good start and also this monopole length is compact enough to be integrated as a wearable antenna. The current behavior was studied, where it is shown in the current distribution behavior of Case 1, in Figure 3A, that the current is a typical monopole antenna, where it is mostly focused on the square's vertical sides, along the y-axis, since this is the axis where the antenna is excited. Since the aim is to design a wearable antenna at 2.45 GHz, the operating frequency had to be reduced along with not increasing the physical size of the antenna. Hence, a study was done on reducing the resonant frequency by increasing the electrical length by cutting slots in the main square radiator. As such, the second step was chamfering a vertical slot at the right edge only of the square shape, referred to as Case 2, as shown in Figure 1B. The simulated EM reflection coefficient in Figure 2B shows that Case 2 antenna resonates at 2.72 GHz. Moreover, its simulated current distribution is shown in Figure 3B, which confirms that it is still compatible with that of typical monopole antenna, which can tell the achievement of the typical monopole radiation pattern.

Similarly, Case 3 antenna shows a chamfered slot in the left edge only of the square shape, as portrayed in Figure 1C, where the antenna resonates at 2.72 GHz too, as shown in Figure 2B, since it is symmetrical over the y-axis. Moreover, its current distribution is shown in Figure 3C, which confirms the same conclusion of the current distribution in Case 2. Finally, slots were chamfered at both edges of the square shape forming the proposed I-shaped antenna, referred to as Case 4, where resonance at 2.45 GHz is attained, as portrayed in Figure 2B. Furthermore, the proposed I-shaped antenna current distribution is shown in Figure 3D, which confirms the same conclusion of the current distribution in Case 2.

It is worth to comment that the position of the slot was based on the current behavior of the conventional square-shaped monopole antenna, where disturbing the current at the square sides directly affects the antenna

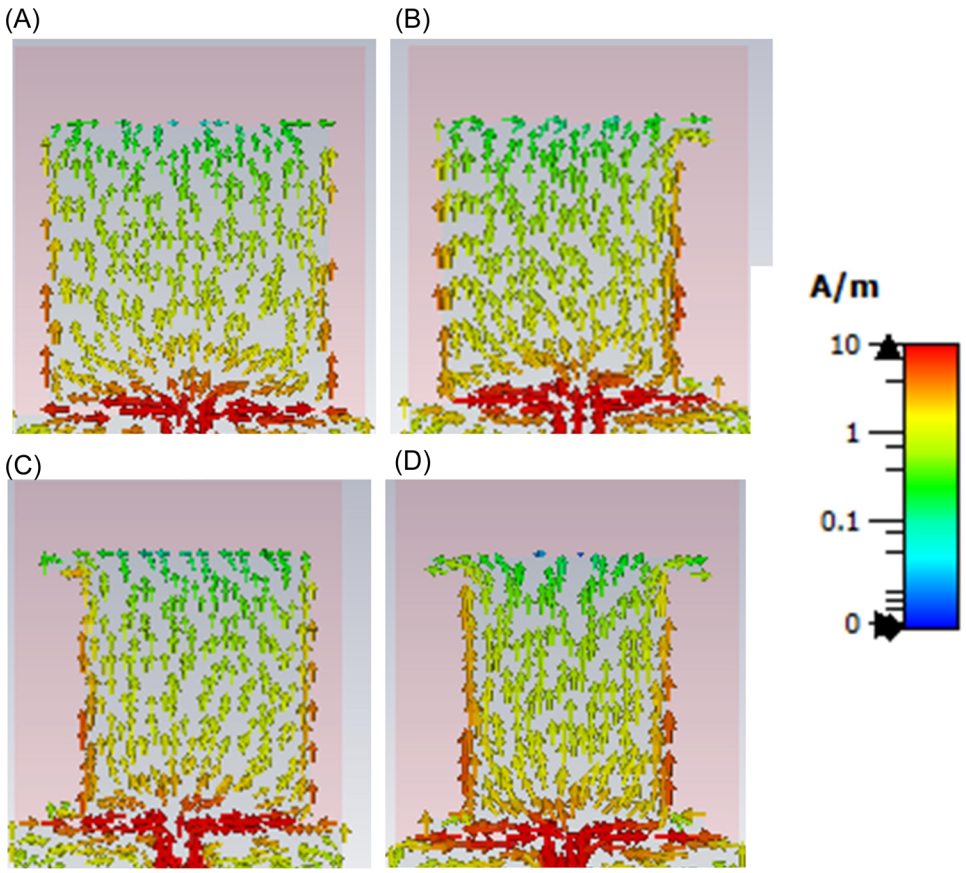

FIGURE 3 The current distribution behavior of each antenna design step: (A) The conventional square-shaped monopole antenna (Case 1); (B) etched right slot antenna (Case 2); (C) etched left slot antenna (Case 3); and (D) the I-shaped antenna (Case 4).

TABLE 1 A parametric study on the effect of slot width on antenna resonance realized gain and radiation efficiency.

Slot width size	Antenna resonance (GHz)	Realized gain (dBi)	Radiation efficiency (%)
2 mm	3.075	0.63	87.45
4 mm	2.84	0.94	88.92
6 mm	2.72	1.13	89.3
8 mm	2.45	1.65	95.5

resonance. The size of the slot was determined by a study conducted on the slot width. Tabulated in Table 1 are the outcomes of this study for the antenna in Figure 1D. It is observed that there is an inversely proportional relation between the slot width and the antenna resonance. By increasing the width of the slot from 2 to 8 mm, the resonant frequency is reduced from 3.1 to 2.45 GHz. In addition, the antenna realized gain and radiation efficiency are enhanced. Hence, the optimum I-shaped antenna dimensions were attained based on reaching the optimum antenna performance.

From the fabrication point of view, ironing was the technique used to integrate the conductive parts into the substrate, since ShieldIt Super possesses an adhesive back that requires small amounts of heat to stick to the dielectric substrate. Illustrated in Figure 4A is the proposed antenna top view including the I-shaped patch dimensions and a close-in view of the dimensions of the CPW feeding arrangement.

After manual fabrication process was finished, the fabricated antenna reflection coefficient was measured, in free space, using Rohde & Schwarz ZVB20 Vector Network Analyzer (VNA), as shown in the inset of Figure 4B. The tested result is benchmarked against the simulated one in Figure 4B. Inspecting Figure 4B, at 2.45 GHz, the simulated result (blue solid) displays matching of −17.5 dB with fractional bandwidth of 19.6%. Conversely, the tested result (dotted red) displays an improved matching of −27 and −10 dB bandwidth of 1.859 GHz. Such discrepancies could be due to human error in fabricating the textile-based antenna, the cold soldering of the SMA connector, and the effect of the non-clean measuring environment. As shown in Figure 5A, the antenna surface current distribution is at the operating frequency of 2.45 GHz. It is clear that the currents are highly clustered along the antenna's vertical sides indicating that a change in the side lengths would affect the antenna resonance. In free space, the antenna displays the conventional 3D omnidirectional radiation pattern, as shown in Figure 5B. It has a simulated realized gain of 1.46 dBi (left scale-solid blue), and radiation efficiency of 90% (right scale-red dotted) at the operating

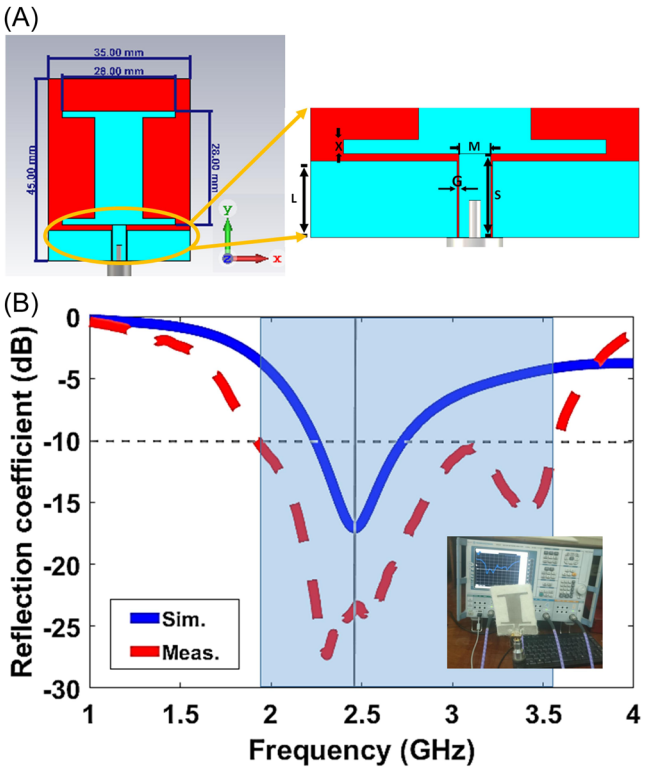

FIGURE 4 (A) The proposed I-shaped textile-based antenna 2D layout ($M = 3.4$ mm, $G = 0.2$ mm, $X = 1.5$ mm, $L = 8.2$ mm, and $S = 9$ mm). (B) Comparison between the simulated and measured reflection coefficients in free space, along with an inset of the measurement setup.

frequency, as highlighted in Figure 5C. Similarly, the human-made antenna radiation pattern was measured inside the anechoic chamber, where the setup is shown in Figure 6A. Portrayed in Figure 6B are the simulated and measured radiation patterns in normalized polar plot representation at the resonant frequency. In free space, the left polar plot is at $\phi = 90°$, where the antenna displays the well-known figure-of-eight. Whereas, the right polar plot is at $\phi = 0°$, where the antenna radiates in equal directions. Clearly, the simulated and measured results highly match and both sets of plots form the monopole-like radiation pattern type.

3 | THE INTEGRATED ANTENNA CONFIGURATION AND FREE-SPACE PERFORMANCE

AMCs arrays aim in isolating the antenna from the human body. However, in free space, the AMC array drastically improves the antenna realized gain. Demonstrated in Figure 7A is top view of the proposed AMC unit-cell structure. The square patch unit-cell was

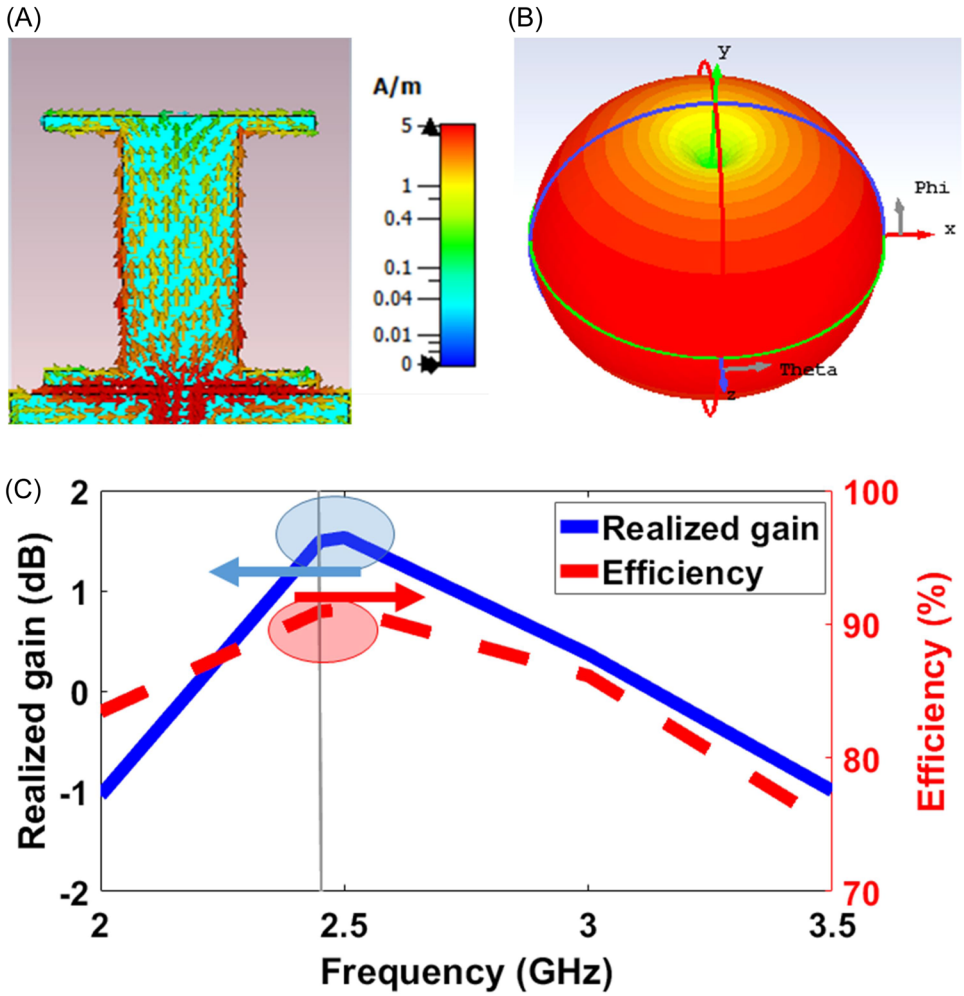

FIGURE 5 The proposed antenna: (A) surface current distribution; radiation properties in free space; (B) 3D realized gain radiation pattern at 2.45 GHz; and (C) simulated realized gain (left-hand scale) and radiation efficiency (right-hand scale) against frequency.

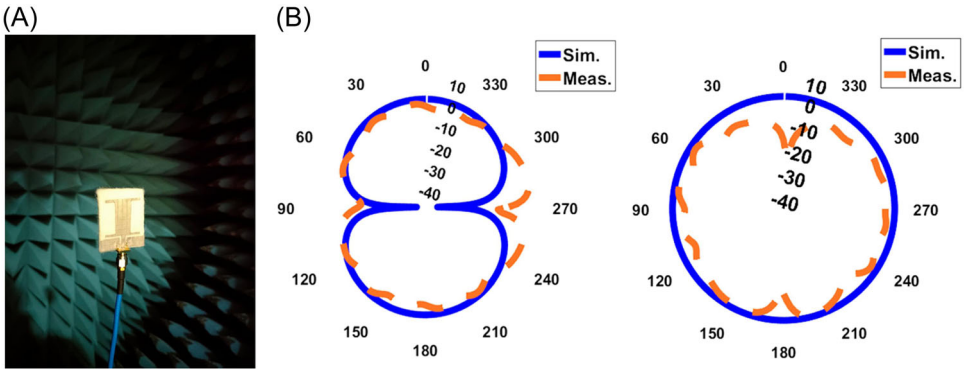

FIGURE 6 (A) The setup for measuring the antenna radiation pattern in free space. (B) Comparison between the simulated and measured normalized 2D polar plot representation of the radiation pattern at 2.45 GHz (left is Y–Z plane, while right is X–Z plane).

designed, where it was slotted at its center by a cross shape of dimensions 2 mm × 20 mm, to maintain compact unit-cell physical size, of 24.6 mm × 24.6 mm (0.2λ × 0.2λ), and achieve reflection phase of 0° at 2.45 GHz. Emphasized in Figure 7B are the unit-cell specifications. The left-hand scale (solid-blue) displays the reflection phase, where 0° is attained at 2.45 GHz. Moreover, the designed unit-cell exhibits a wide bandwidth that ranges from 1.44 GHz at −90° to 2.75 GHz at +90°. Finally, another property of AMC is high

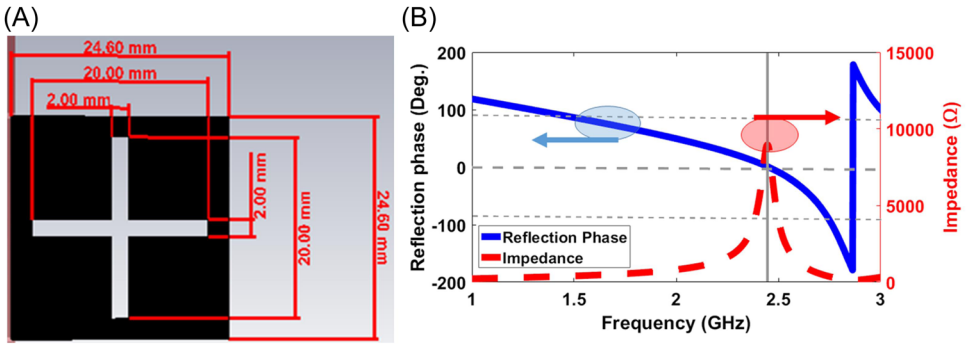

FIGURE 7 (A) 2D layout of the proposed AMC unit-cell structure. (B) The AMC unit-cell characteristics, where the left scale indicates the reflection phase and the right scale refers to the impedance, against frequency. AMC, artificial magnetic conductor.

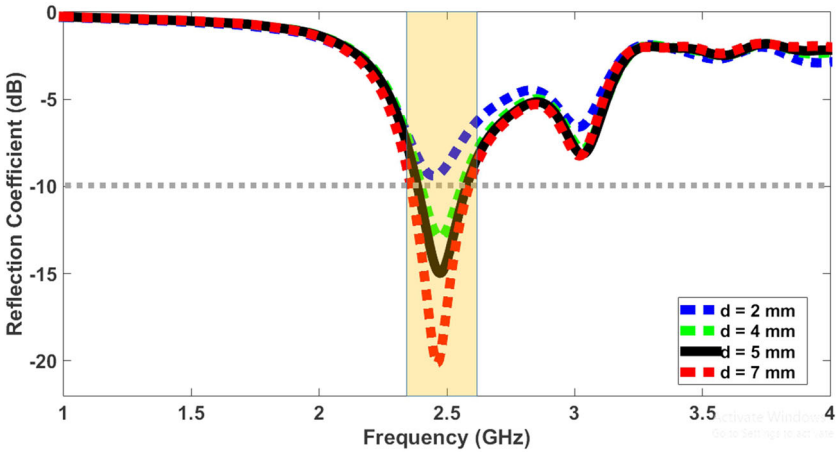

FIGURE 8 A parametric study in term of S_{11} on the separation in-beween the antenna and AMC in free space. AMC, artificial magnetic conductor.

TABLE 2 A parametric study in terms of realized gain and radiation efficiency on the separation in-between the antenna and AMC in free space at 2.45 GHz.

Distance	Realized gain (dBi)	Radiation efficiency (%)
2 mm	5.43	58.93
4 mm	6.29	68.72
5 mm	6.57	72.22
7 mm	6.90	77.30

Abbreviation: AMC, artificial magnetic conductor.

impedance, where a value of 8.88 kΩ is achieved at 2.45 GHz, as represented in Figure 7B right-hand scale (dotted-red).

The textile-based antenna and textile-based AMC array are separated by 5 mm of foam to form the integrated antenna. To decide on that specific separation, a parametric study was conducted on the separation in-between the antenna and AMC. The different separations that were studied were 2, 4, 5 (proposed), and 7 mm. The studies included a comparison with respect to S_{11}, where the outcome is plotted in Figure 8. As observed in Figure 8, the antenna maintains its 2.45 GHz resonance at all separations and the matching is improved with the increase in separation. Moreover, a comparison in terms of the antenna realized gain and radiation efficiency in free space at 2.45 GHz has been included in Table 2. Studying the achieved numbers, the antenna performance parameters are improved as the separation increases; however, it is worth noting that a separation higher than 5 mm would increase the overall integrated antenna design (antenna and AMC) volume. This is not suitable since the aim is to design a compact integrated antenna design (antenna and AMC). Hence, a compromise had to be done between size and antenna performance parameters; therefore, the distance of 5 mm was chosen as the optimum separation.

The top view of the integrated antenna layout is revealed in Figure 9A. Benchmarked against one another in Figure 9B is the simulated and tested S_{11}. At 2.45 GHz, the simulated result (blue solid) displays matching of −15 dB with fractional bandwidth of 19.6%. Whereas, the tested result (dotted red) displays an almost equal matching of −15 dB and maintains its −10 dB wide

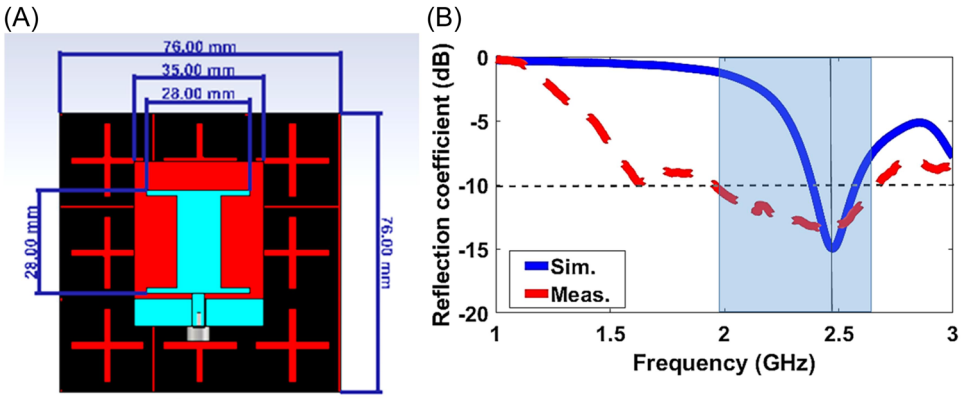

FIGURE 9 (A) The proposed integrated fully textile-based antenna 2D layout. (B) Comparison between the integrated antenna simulated and measured reflection coefficients in free space.

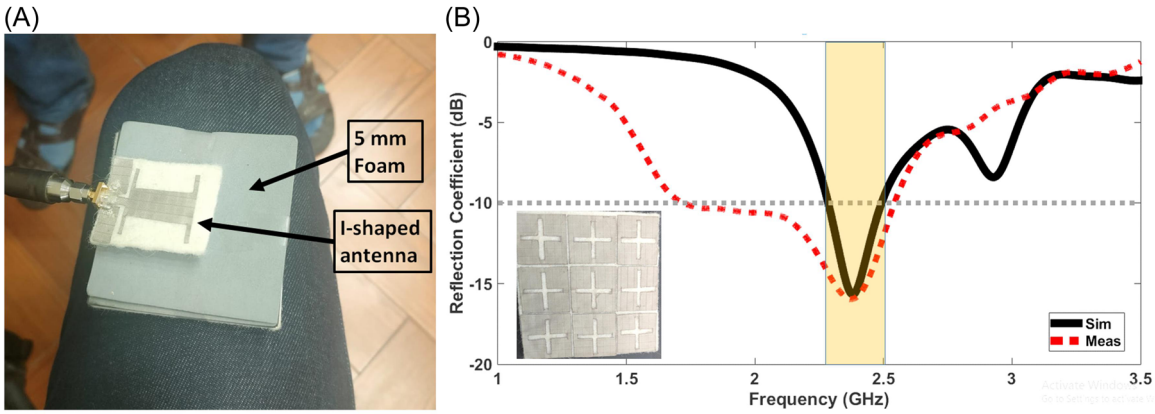

FIGURE 10 (A) The setup for measuring the proposed integrated fully textile-based antenna reflection coefficient. (B) Comparison between the integrated antenna simulated and measured reflection coefficients on the human body, along with an inset of the fabricated 3×3 AMC array structure. AMC, artificial magnetic conductor.

bandwidth that extends from 2 to 2.6 GHz. As stated in the previous section, such differences could be attributed to manual errors in fabrication.

4 | THE INTEGRATED ANTENNA PERFORMANCE OVER HUMAN MODEL

The aim of the designed antenna is to apply it in wearable uses, as such, displayed in Figure 10A is the setup for measuring the proposed integrated antenna reflection coefficient on the human thigh. The presented I-shaped antenna is spaced from the AMC structure by a 5-mm-thick foam, as pointed out in the previous section. A comparison between the simulated and measured outcomes is plotted in Figure 10B. The results highly match in terms of antenna resonance at 2.45 GHz with a similar matching level of −16 dB. However, the measured result displays a wider fractional bandwidth, which could be due to a number of factors. Such influences include human error in fabricating the textile-based antenna, the cold soldering of the SMA connector, and the effect of the non-clean measuring environment. It is worth noting that an inset of the fabricated 3×3 AMC array structure, which has a footprint of 76 mm × 76 mm ($0.62\lambda \times 0.62\lambda$), is included in Figure 10B, since it is covered by the foam in Figure 10A.

The SAR result should be considered to ensure that the proposed integrated antenna is suitable for wearable applications. Accordingly, illustrated in Figure 11A is the setup for evaluating SAR. The integrated antenna is backed by a three-layered model that imitates the human main tissues of skin, fat, and muscle, respectively. The human tissue model thickness is subdivided into 2 mm of skin, followed by 8 mm of fat, and then 23 mm of muscle.

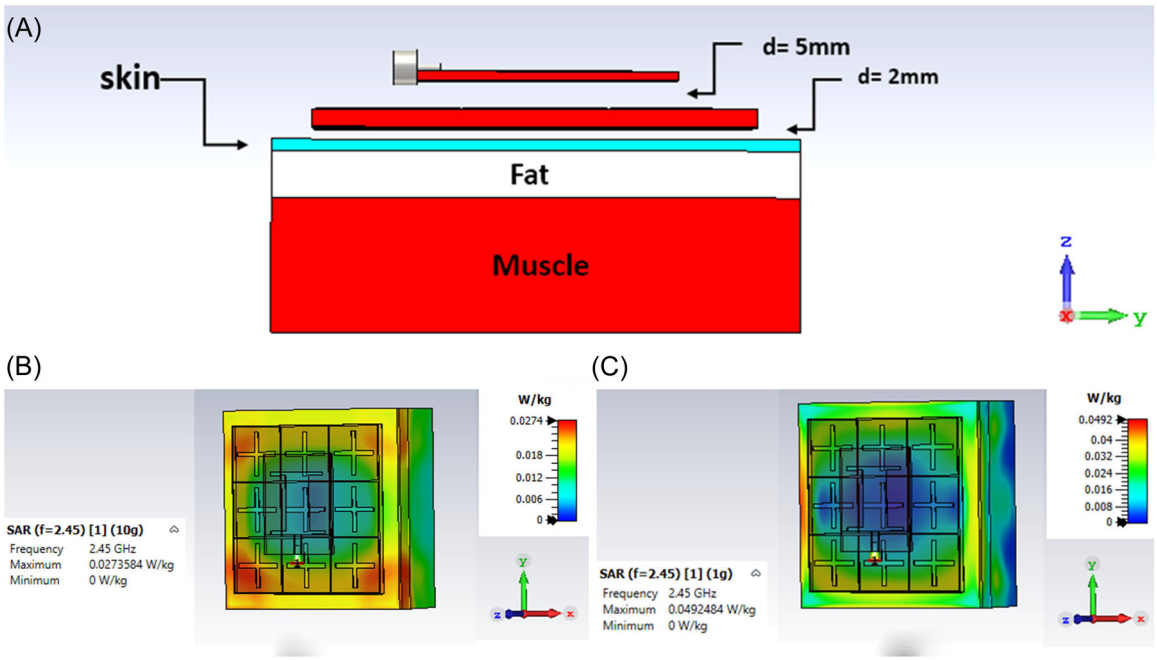

FIGURE 11 (A) Side-view of the proposed integrated fully textile-based antenna over a human-body model; (B) the integrated antenna maximum SAR value averaged over 10 g of tissue; and (C) the integrated antenna peak SAR value averaged over 1 g of tissue. SAR, specific absorption rate.

TABLE 3 Effect of the AMC reflector on the antenna SAR results averaged over 1 g and 10 g of tissue at 2.45 GHz.

Tissue mass	Maximum antenna SAR without AMC (W/kg)	Maximum integrated antenna SAR (W/kg)
1 g	46.35	0.049
10 g	18.20	0.027

Abbreviations: AMC, artificial magnetic conductor; SAR, specific absorption rate.

The conductivity, permittivity, and mass density of the human tissue layers are found in refs. [18–20], where the human tissue dielectric properties are frequency-dependent.

In simulation, the antenna input power is fixed at 100 mW, which was selected for fair comparison with the reported literature. As shown in Figure 11B,C, the achieved SAR value, where the attained maximum SAR value, averaged over 10 g of tissue, is 0.0274 W/kg which is by far lower than the 2 W/kg limit. In addition, averaged over 1 g of tissue, the accomplished peak SAR value is 0.0492 W/kg, which is, similarly, lower than the 1.6 W/kg level.

A similar experiment was conducted without the AMC, where the I-shaped antenna was placed above the three-layered human model and the SAR results were studied. Tabulated in Table 3 are the SAR results of the antenna without the AMC and with the AMC for comparison purposes. As observed, in the absence of the AMC, the SAR results are very high and exceed the EU and American standards. However, after adding the AMC, the integrated antenna displays very low SAR results with almost 99% reduction. These inferior values are obtained due to the incorporated AMC array reflector, which allows the antenna to operate at close distances to the human body without highly affecting the human health.

Finally, a comparison between the presented antenna, with and without the AMC array, against some reported literature, at the same operating frequency, is tabulated in Table 4. Different comparison criteria include the antenna and AMC physical sizes, the antenna electrical size, the antenna realized gain and radiation efficiency parameters, in free space and against the human body, along with the maximum simulated SAR level. The used substrate is thinner than refs. [5–7]; hence, ensuring high degree of flexibility. The incorporated AMC size is more compact than refs. [3, 6, 7], which is desired for wearable applications. The antenna realized gain in free space is higher than ref. [2]. The integrated antenna realized again against the human body is higher than [2] and [12]. The antenna by itself and the integrated antenna, including the AMC, radiation efficiencies are the highest despite the low thickness. Finally, the SAR level is lower than the references

TABLE 4 Comparison between the introduced I-shaped antenna and other-related work in free space and against the human body at 2.45 GHz.

References	Antenna physical size (mm^2)	Antenna electrical size in terms of free-space wavelength (λ_0) at the lowest frequency	Substrate type/thickness (mm)	Reflector physical size (mm^2)/type	Realized gain (dBi) in free space	Realized gain (dBi) against human body (including reflector)	Rad. efficiency (%) in free space	Rad. efficiency (%) against human body (including reflector)	Max. SAR (W/kg) at input power of 100 mW
[2]	30 × 25	$0.24\lambda_0 \times 0.20\ \lambda_0$	Polyimide/0.05	74 × 74/metasurface	1.25	5.2	82.3	61.3	2.48
[3]	N/A	N/A	Polyester Film/0.1	135 × 135/EBG	3.41	7.93	N/A	N/A	0.07
[4]	30 × 20	$0.24\lambda_0 \times 0.16\lambda_0$	Denim/0.7	46 × 46/EBG	N/A	7.8	N/A	N/A	0.04
[5]	32 × 39	$0.26\lambda_0 \times 0.31\lambda_0$	Felt/2	50 × 75/AMC	1.97	N/A	N/A	44	0.86
[6]	32.1 × 57	$0.26\lambda_0 \times 0.47\lambda_0$	Pellon/3.6	124 × 124/AMC	2.45	8.4	95	66	0.33
[7]	40 × 32	$0.32\lambda_0 \times 0.26\lambda_0$	Felt/2	81 × 81/EBG	3.5	N/A	55	N/A	0.55
[12]	21 × 33	$0.17\lambda_0 \times 0.27\lambda_0$	PDMS/1.5	50 × 50/metasurface	N/A	5.1	N/A	68	0.2
Proposed	35 × 45	$0.28\lambda_0 \times 0.36\lambda_0$	Felt/1.5	76 × 76/AMC	1.65	6.57	95.5	84.26	0.05

compared to in Table 4 and is almost equal to ref. [4], the proposed integrated antenna presents results that are highly competitive and surpass some of the published literature, which highly suggests that the antenna is suitable for wearable uses; such as monitoring the health status of patients suffering from diabetes, tested on the thigh, by using a noninvasive wearable instrument, as in ref. [15].

5 | CONCLUSION

An integrated antenna, composed of an I-shaped CPW-fed antenna and a 3 × 3 AMC array, acting as a reflector, was presented. The integrated antenna is based on textile materials; hence, achieving both low thickness and flexibility, and functions at 2.45 GHz; thus, serving the medical sector of the various wearable applications. As a result of backing the antenna with the reflecting structure, high gain values of 6.57 dB, in free space, and 6.2 dB, over the human body model, were attained, at the operating frequency. Finally, the I-shaped antenna displayed a peak SAR level of 46.35 W/kg, over 1 g of tissue, which was reduced to 0.05 W/kg, after combining the AMC array. Because of the textile-based integrated antenna traits and outcomes, it is highly advised for 2.45 GHz wearable and medical uses.

DATA AVAILABILITY STATEMENT

The data that support the findings of this study are available from the corresponding author upon reasonable request.

ORCID

Mahmoud A. Abdalla https://orcid.org/0000-0001-6759-7268

REFERENCES

1. Hall PS, Hao Y. *Antennas and Propagation for Body-Centric Wireless Communications*. Artech House; 2012.
2. Wang M, Yang Z, Wu J, et al. Investigation of SAR reduction using flexible antenna with metamaterial structure in wireless body area network. *IEEE Trans Antennas Propag*. 2018;66(6):3076-3086.
3. Abirami BS, Sundarsingh EF. EBG-backed flexible printed Yagi-Uda antenna for on-body communication. *IEEE Trans Antennas Propag*. 2017;65(7):3762-3765.
4. Ashyap AYI, Zainal Abidin Z, Dahlan SH, et al. Compact and low-profile textile EBG-based antenna for wearable medical applications. *IEEE Antennas Wirel Propag Lett*. 2017;16:2550-2553.
5. Mersani A, Osman L, Ribero J-M. Performance of dual-band AMC antenna for wireless local area network applications. *IET Microw Antennas Propag*. 2018;12(6):872-878.
6. Alemaryeen A, Noghanian S. Crumpling effects and specific absorption rates of flexible AMC integrated antennas. *IEEE Trans Antennas Propag*. 2019;67(6).

7. Gao G-P, Hu B, Wang S-F, Yang C. Wearable circular ring slot antenna with EBG structure for wireless body area network. *IEEE Antennas Wirel Propag Lett*. 2018;17(3):434-437.
8. Gao GP, Yang C, Hu B, Zhang RF, Wang SF. A wide-bandwidth wearable all-textile PIFA with dual resonance modes for 5 GHz WLAN applications. *IEEE Trans Antennas Propag*. 2019;67(6):4206-4211.
9. Ashyap AYI, Dahlan SHB, Abidin ZZ, et al. Fully fabric high impedance surface-enabled antenna for wearable medical applications. *IEEE Access*. 2021;9:6948-6960.
10. Li H, Sun S, Wang B, Wu F. Design of compact single-layer textile MIMO antenna for wearable applications. *IEEE Trans Antennas Propag*. 2018;66(6):3136-3141.
11. El Atrash M, Abdalla MA, Elhennawy HM. A compact highly efficient Π-section CRLH antenna loaded with textile AMC for wireless body area network applications. *IEEE Trans Antennas Propag*. 2021;69(2):648-657.
12. Jiang ZH, Cui Z, Yue T, Zhu Y, Werner DH. Compact, highly efficient, and fully flexible circularly polarized antenna enabled by silver nanowires for wireless body-area networks. *IEEE Trans Biomed Circuits Syst*. 2017;11(4):920-932.
13. Simorangkir RBVB, Kiourti A, Esselle KP. UWB wearable antenna with a full ground plane based on PDMS-embedded conductive fabric. *IEEE Antennas Wirel Propag Lett*. 2018;17:493-496.
14. Singh S, Verma S. SAR reduction and gain enhancement of compact wideband stub loaded monopole antenna backed with electromagnetic band gap array. *Int Journal RF Microw Comput Aided Eng*. 2021;31(10):1-11.
15. El Atrash M, Abdalla MA, Elhennawy HM. A wearable dual-band low profile high gain low SAR antenna AMC-backed for WBAN applications. *IEEE Trans Antennas Propag*. 2019;67:6378-6388.
16. El Atrash M, Abdalla MA, Elhennawy HM. Gain enhancement of a compact thin flexible reflector-based asymmetric meander line antenna with low SAR. *IET Microw Antennas Propag*. 2019;13(6):827-832.
17. Sambandam P, Kanagasabai M, Ramadoss S, et al. Compact monopole antenna backed with fork-slotted EBG for wearable applications. *IEEE Antennas Wirel Propag Lett*. 2020;19(2):228-232.
18. Dielectric Properties of Body Tissues [online]. http://niremf.ifac.cnr.it/tissprop/
19. Body Tissue Dielectric Parameters [online]. https://www.fcc.gov/general/body-tissue-dielectric-parameters
20. Density and Mass of Each Organ Tissue [online]. http://bionumbers.hms.harvard.edu/bionumber.aspx?id=110245

How to cite this article: Youssef OM, Atrash M, Abdalla MA. A compact fully fabric I-shaped antenna supported with textile-based AMC for low SAR 2.45 GHz wearable applications. *Microw Opt Technol Lett*. 2023;1-10. doi:10.1002/mop.33647